Published in final edited form as:

Mol Pharm. 2019 October 07; 16(10): 4302–4312. doi:10.1021/acs.molpharmaceut.9b00639.

Development of MicroRNA-146a-Enriched Stem Cell Secretome for Wound-Healing Applications

Renae Waters, **Siddharth Subham**, **Settimio Pacelli**, **Saman Modaresi**, **Aparna R. Chakravarti**, **Arghya Paul**[*,†]

BioIntel Research Laboratory, Department of Chemical and Petroleum Engineering, School of Engineering, University of Kansas, Lawrence, Kansas 66045, United States

Abstract

Secretome-based therapies have the potential to become the next generation of viable therapeutic wound repair treatments. However, precise strategies aimed to refine and control the secretome composition are necessary to enhance its therapeutic efficacy and facilitate clinical translation. In this study, we aim to accomplish this by transfecting human adipose-derived stem cells (hASCs) with microRNA-146a, which is a potent regulator of angiogenesis and inflammation. The secretome composition obtained from the transfected hASCs (secretome^{146a}) was characterized and compared to nontransfected hASCs secretome to evaluate changes in angiogenic and anti-inflammatory growth factor, cytokine, and miRNA content. In vitro proliferation, migration, and tubular morphogenesis assays using human umbilical vein endothelial cells (HUVECs) were completed to monitor the proangiogenic efficacy of the secretome^{146a}. Finally, the anti-inflammatory efficacy of the secretome^{146a} was assessed using HUVECs that were activated to an inflammatory state by IL-1β. The resulting HUVEC gene expression and protein activity of key inflammatory mediators were evaluated before and after secretome treatment. Overall, the secretome^{146a} contained a greater array and concentration of therapeutic paracrine molecules, which translated into a superior angiogenic and anti-inflammatory efficacy. Therefore, this represents a promising strategy to produce therapeutic secretome for the promotion of wound repair processes.

Graphical Abstract

[*]**Corresponding Author**: arghya.paul@uwo.ca.

[†]**Present Address**: A.P.: Department of Chemical and Biochemical Engineering, Department of Chemistry, The University of Western Ontario, London, ON N6A 5B9, Canada

Supporting Information

The Supporting Information is available free of charge on the ACS Publications website at DOI: 10.1021/acs.molpharmaceut.9b00639. Reporting western blot raw data, flow cytometry analysis proving the interaction of HUVECs with EVs, actin DAPI staining of HUVECs cultured on Matrigel in the presence of different types of the secretome, as well as CD31 staining of HUVECs (PDF)

The authors declare no competing financial interest.

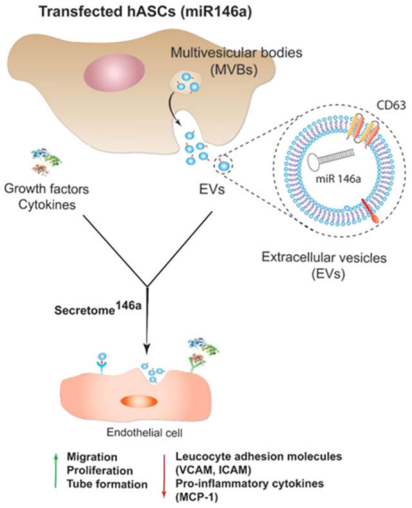

Keywords

angiogenesis; anti-inflammatory agents; extracellular vesicles; microRNA; secretome

1. INTRODUCTION

Wound healing is a well-organized process comprised of three temporally and spatially overlapping phases, including inflammatory, proliferative or the formation of granular tissue, and remodeling or scar formation. In the case of acute wounds, this process typically leads to the re-establishment of the tissue integrity; however, diabetic and elderly patients often suffer from complications due to chronic wounds that do not heal. In the United States, the cost associated with the care of chronic wounds exceeds 1 billion dollars and is anticipated to significantly increase with the predicted number of adults 65 years or older almost doubling by 2030 and the increased prevalence of diabetic children. To address this clinical need, scientists have focused their efforts on using exogenous stem cells as a strategy to regulate the wound-healing cascade and promote effective healing.

To accomplish this goal, multiple adult stem cell types have been used in clinical and preclinical studies based on the hypothesis that stem cells would induce the formation of a new functional tissue upon long-term engraftment at the wound site.[1–4] However, this hypothesis does not align with the results reported in several preclinical and small-scale clinical trials because of the limited stem cell retention, engraftment, and transdifferentiation observed in these studies.[5] Based on this evidence, the positive therapeutic effect has been primarily attributed to the secretion of therapeutic paracrine molecules that promote endogenous reparative and regenerative responses at the wound site. This pivotal discovery has led to a significant effort in identifying novel cell-free treatments, which are based on the delivery of key angiogenic, antiapoptotic, anti-inflammatory, and antifibrotic paracrine factors. This milieu of therapeutic factors, known as secretome, has been proven to be effective in promoting an intrinsic regenerative response at the wound site by modulating endogenous cell function and influencing wound closure.[6–9] Recent studies include the use

of the secretome obtained from various cell lines. For instance, secretome derived from bone marrow-derived mesenchymal stem cells (MSCs) has been reported to improve renal function after induced renal ischemia in vivo.[10] Additionally, skin-derived multipotent stromal cell secretome was able to promote angiogenesis in a preclinical mouse model of cutaneous wound healing,[11] whereas γ-irradiated peripheral blood mononuclear cell-derived secretome was effective in accelerating wound closure in a diabetic mouse model and in a porcine model of acute burn wounds.[12,13] In addition, we have previously demonstrated that secretome produced by MSC spheroids was able to induce angiogenesis, which is an integral part of the proliferative phase of wound healing.[14,15]

The secretome is a complex array of pleiotropic molecules secreted by stem cells, which includes growth factors, cytokines, miRNA, and extracellular vesicles (EVs).[13,16,17] Specifically, EVs are small bilayered particles that were originally identified as a strategy for stem cells to discard the undesired cellular material. However, in recent studies, EVs have been identified as regulators of cell to cell communication by carrying essential paracrine factors.[18–22] There are two types of EVs regularly secreted by healthy cells. The first type is known as exosomes (30–150 nm) and the second type is defined as microvesicles, which possess a broader size distribution (100–1000 nm). Both types of EVs are composed of a phospholipid bilayer membrane containing ligand receptors and major histocompatibility complex molecules, which facilitate binding to cell receptors that are necessary to trigger signaling cascades within the target cell. In addition, EVs have also been shown to transport an array of RNA types, including messenger RNA (mRNA),[23,24] and, of particular note, miRNA.[16,23,25] miRNA are small (21–23 nucleotides), endogenous, noncoding RNAs that negatively regulate gene expression on a post-transcriptional level and act as powerful regulators of pathophysiological processes.[26] In the context of wound-healing applications, stem cell-derived EVs have been shown to promote angiogenesis, modulate inflammation, inhibit apoptosis, and induce proliferation due to the presence of specific miRNA loaded within their bilayer structure.[18,27–29] Precisely, among the different types of miRNA, miR-146a has been shown to be a potent regulator of inflammation[30,31] in addition to its ability to promote angiogenesis and inhibit cardiomyocyte apoptosis.[32,33] Based on these studies, it is evident that optimizing the miRNA composition within EVs represents an innovative strategy to develop a cell-free therapeutic treatment that exhibits a greater therapeutic efficacy for wound-healing applications.

In this study, we aimed to enhance the therapeutic efficacy of human adipose-derived stem cells (hASCs)-derived secretome by transfecting the cells with miR-146a to induce the secretion of EVs carrying this therapeutic miRNA. The hypothesis was that the presence of the miR-146a within the EVs would cause an increase in the proangiogenic and anti-inflammatory response of the secretome in comparison to the one produced by hASCs that were not transfected. To test this hypothesis, the angiogenic and anti-inflammatory growth factor, cytokine, and miRNA composition of the two types of the secretome were compared to identify changes in the therapeutic paracrine molecule composition after transfection. Finally, the angiogenic and anti-inflammatory properties of the two different types of the secretome were tested and compared in vitro by evaluating their modulation on endothelial cell proliferation, migration, tube formation, inflammatory activation, gene expression, and protein activity.

2. MATERIALS AND METHODS

2.1. hASCs Culture Conditions and Transfection with miR-146a.

hASCs isolated from female donors (31–45 years old) were purchased from Rooster Bio. Passages 2–6 were used for all the experiments, and cells were cultured in traditional 2D conditions (3.3×10^3 cells/cm^2) using hASCs High-performance media (Rooster Bio media) at 37 °C and 5% CO_2.

hASCs were seeded in 6 well plates (1×10^5 cells/well) and cultured for 24 h in Rooster Bio media containing 10% of fetal bovine serum (FBS). Upon 70% of confluency, cells were washed three times with phosphate buffer saline (PBS) at pH 7.4. The media was then switched to the endothelial growth medium (EGM-2 BulletKit, Lonza), without the addition of FBS and angiogenic growth factors including the vascular endothelial growth factor (VEGF) and human fibroblast growth factor-B (hFGF-B). hASCs were then transfected with the XMIR-146a-5p RNA Oligo (10 μM) (System Bioscience) using the Purefection Transfection Reagent (System Bioscience). Specifically, 30 μL of the oligonucleotide suspension and 7.5 μL of the transfection reagent were mixed prior addition to the cells in 200 μL of Dulbecco's modified Eagle's medium media without any FBS. The mixture was vortexed briefly and incubated at room temperature for 15 min. Then, the complex was added to the cells to reach a final concentration of 100 nM of oligonucleotide in each well. The well plate was kept on a shaker incubator for 30 min followed by incubation at 37 °C for 24 h according to the manufacturer's protocol. As a control group, hASCs were treated in the same culture conditions without being transfected with the oligonucleotide miR-146a. The media was collected from both groups, centrifuged at 16 000*g* for 10 min at 4 °C to remove cellular debris, and used fresh or stored at −20 °C for further analysis.

2.2. EV Isolation from Transfected Cells and Morphological Characterization.

The secretome^{146a} and the control group (secretome) were collected, as reported in the previous section. After centrifugation, the exosomes were isolated using the exoEasy Maxi Kit (Qiagen). Briefly, the supernatant was mixed with an equal volume of the XBP buffer (Qiagen) and centrifuged at 500*g* for 1 min, followed by subsequent washing steps according to the manufacturer's protocol. The isolated exosomes were retrieved in the XE elution buffer in a final volume of 400 μL.

Exosomes morphological analysis was carried out by transmission electron microscopy (TEM). TEM samples were prepared by adding 5 μL of the exosome sample onto the carbon-coated 200 mesh copper grids for 5 min to allow the exosomes to adsorb to the surface. The grids were dried for several hours in a desiccator. The dried grids were analyzed with a Philips CM100 microscope operated at 100 kV. High-resolution TEM images were recorded using an FEI Tecnai F20XT, 200 kV (FEI, Hillsboro, OR).

Finally, the exosome size distribution and concentration were assessed by the nanoparticle tracking analysis (NTA) using a Malvern Panalytical NanoSight LM10. Exosomes samples were suspended in PBS and injected into the sample chamber using sterile syringes. The samples were loaded by filling the chamber without the introduction of air bubbles. The detection threshold was fixed to 60 particles per field of view, and the camera level was set

in the standard mode. All measurements were performed in triplicate at room temperature with every measurement lasting for 1 min. The concentration values and the particle sizes were determined using the NanoSight software.

2.3. Western Blot Analysis of Isolated EVs.

Western blot analysis was carried for both the exosomes and the cell lysates samples to verify the presence of specific protein markers in the exosome population. hASCs were cultured following the cell culture conditions described in Section 2.1, and the exosomes were isolated based on the procedure described previously in Section 2.2. The cell lysate was prepared by treating hASCs with radio immunoprecipitation assay buffer containing Tris–HCl (pH 7.6, 25 mM), NaCl (150mM), NP-40 (1% w/v), sodium deoxycholate (1% w/v), and sodium dodecyl sulfate (0.1% w/v). The protein concentration was determined by measuring the optical density at 280 nm using a spectrophotometer (Nanodrop ND-1000; Thermo Scientific). The exosomes samples were normalized using the same sample volume in the precasted gel for western blot analysis (29 μL).

The protein samples (80 μg of the cell protein or 29 μL of exosomes in each well) were resolved by sodium dodecyl sulfate polyacrylamide gel electrophoresis (BoltTM 4–12% Bis-Tris Plus) at 180 V for 42 min. The proteins bands were transferred to Poly(vinylidene difluoride) membranes (Immobilon-P Transfer Membranes), blocked in 0.5% Tween 20, and probed with antibodies, which were diluted in the corresponding blocking buffer. The cellular protein cytochrome *c* was resolved under reducing conditions, whereas the exosome protein CD63 was resolved under nonreducing conditions. The antibodies used were anti-CD63 antibody (ab59479) dilution 1:2000 and anti-cytochrome *c* antibody (ab110325) dilution 1:2000 in the blocking buffer. Goat anti-Mouse IgG H&L (HRP) (ab205719) was used as the secondary antibody at dilution of 1:4000. The protein band signals were detected using an X-ray film and enhanced by a chemiluminescent reagent. The signals were detected using an ECL Plus detection system according to the manufacturer's protocol.

2.4. EVs Internalization Study into Human Umbilical Vein Endothelial Cells (HUVECs).

EVs were isolated following the procedure reported in Section 2.2. Aldehyde/sulfate latex beads were used to conjugate the EVs prior to flow cytometry analysis. Precisely, the beads at the concentration of 5.5×10^6 particles/mL were incubated with EVs at room temperature for 2 h. Subsequently, a solution made of 0.1% bovine serum albumin (BSA), 0.01% of sodium azide in phosphate buffer (BCB) was added to the sample and incubated overnight on a shaker. The samples were centrifuged at 2000*g* for 10 min and washed with BCB buffer. Finally, the pellet consisting of EVs conjugated with the beads was resuspended with BCB for further analysis. EVs-beads suspension (100 μL) was incubated with CD63 primary antibody (ab59479) at a concentration of 10 μg/mL for 1 h at 4 °C on a shaker. Samples were centrifuged at 3000*g* for 10 min and washed with PBS. Finally, a secondary antibody Goat anti-Mouse IgG tagged with the fluorescent dye Alexa Fluor 488 was added to the samples for 1 h on a shaker (1:400 dilution). Samples were centrifuged at 3000*g* for 10 min three times prior to analysis with flow cytometry analysis. Beads without EVs and stained for CD63 were used as a control.

EVs stained with CD63 were also supplemented in the culture medium of HUVECs to evaluate the process of internalization. Cells were incubated with EVs-CD63-stained samples for 24 h at 37 °C. HUVECs were washed with Lonza media EGM-2 bullet kit for three times. Finally, HUVECs were collected by trypsinization and analyzed by flow cytometry analysis. HUVECs that did not undergo any treatment were used as a control group.

2.5. miRNA Analysis of Isolated EVs.

Exosomes isolated from the transfected and the nontransfected groups, as reported in section 2.2, were assessed to evaluate their miRNA content and composition. miRNA was isolated from the exosomes using the exoRNeasy Serum/Plasma Maxi Kit (Qiagen). The total RNA concentration and purity were determined by measuring the optical density at 260 nm using a spectrophotometer (Nanodrop ND-2000; Thermo Scientific). Complementary DNA (cDNA) was synthesized, starting from the isolated RNA using the miScript II RT Kit (Qiagen). The quantitative polymerase-chain-reaction (qPCR) analysis was performed in triplicate for each test group on a Mastercycler Realplex4 (Eppendorf) using predesigned primers and miScript SYBR Green PCR Kit (Qiagen). Fold expression levels of miR-146a in the transfected group (secretome^{146a}) were calculated using the relative ΔΔCt method, using *RNU6* as the housekeeping gene. Similarly, following the same protocol, qPCR analysis was carried out using a miSCript miRNA PCR array 96 well plate (Qiagen) to detect the composition of the miRNA present in the exosomes samples upon transfection compared to the nontransfected group.

2.6. Assessment of Transfected Cell-Derived Secretome Protein Composition.

The secretome obtained from the transfected (secretome^{146a}) and nontransfected hASCs (secretome) was assessed using a human angiogenesis antibody array and human cytokine array (R&D Systems). The two arrays were used to detect the differences in composition between the two different types of the secretome by analyzing the relative levels of 55 angiogenic related proteins and 36 different cytokines, chemokines, and acute-phase proteins. The studies were carried out according to the manufacturer's protocols. Images of the corresponding chemiluminescent dot blots were taken, and the mean spot pixel density for each protein was calculated using the ImageJ software.

2.7. HUVEC Proliferation Assay with Secretome^{146a}.

Angiogenic studies were carried out to assess the superior proangiogenic ability of the secretome^{146a}. Immortalized HUVECs were cultured in the endothelial basal medium EGM-2 BulletKit (Lonza), 2% FBS, and 1% penicillin/streptomycin with complete endothelial growth supplements. HUVECs from passage 2–5 were used in all of the in vitro angiogenic studies. HUVECs (0.2×10^5 cells/mL) were seeded in a 48-well plate and cultured overnight in EGM-2 media, without the addition of FBS and angiogenic growth factors, VEGF and hFGF-B. The cells were then washed with PBS, and the media was replaced with media supplemented with different types of the secretome, as described in Section 2.1. Precisely, three groups were tested: a negative control consisting of HUVECs cultured in EGM-2 media without growth factors (Ctrl (−)), endothelial cells cultured in the same media supplemented with secretome isolated from nontransfected hASCs (secretome),

and a test group where the media without growth factors was supplemented with secretome isolated from transfected hASCs (secretome^{146a}) (n = 5). The final volume in each well was 200 μL, and the volume of the secretome for both test group was 100 μL. HUVEC proliferation within the three groups was determined using an MTS proliferation assay (Promega) and standard calibration curve in the range of 5×10^3 up to 1×10^5 cells after 24 h. The absorbance measurements were carried out at 490 nm, according to the manufacturer's protocol.

2.8. HUVEC Migration and Tube Formation Assay with Secretome^{146a}.

HUVECs (3×10^5 cells/mL) were seeded in Ibidi 3-well culture inserts within a 24-well plate as per the company's protocol to perform a cell migration assay (n = 3). Specifically, 70 μL of the cell suspension was added to each well, and the cells were allowed to culture overnight in EGM-2 media. Next, the inserts were removed, and the media was changed according to the same groups used in the proliferation assay reported in the previous section. Bright-field images were taken in the same positions along the scratch at 0, 6, and 24 h after treatment to monitor HUVECs migration into the gap for each group. The ImageJ software was used to quantify the percentage of area recovered due to cell migration within 10 images per group. The area of the original gap was determined from the initial images taken at the beginning of the study.

Finally, the formation of tubular-like structures by HUVECs seeded on a growth factor-depleted Matrigel was assessed using the manufacturer's protocol after treatment (Matrigel matrix, Basement Membrane, BD). Specifically, growth factor-depleted Matrigel Matrix (289 mL, 10 mg/mL) cooled to 5 °C was added to a 24-well culture plate on ice. The matrix was allowed to form a gel by incubating the plate at 37 °C for 60 min prior to being seeded with HUVECs (1.2×10^5 cells/mL) and treated with one of the same three treatment groups used for the proliferation and migration assays. Bright-field images of the endothelial cell networks were taken after 10 h. Additionally, actin and 4′,6-diamidino-2-phenylindole (DAPI) staining were carried out to visualize the network structure for the different groups. Cells were fixed in 4% of paraformaldehyde for 10 min followed by a permeabilization step with triton 0.1X for 20 min. Actin fibers were stained with Phalloidin conjugated with Alexa Fluor 488, and DAPI was used to visualize the nuclei of the cells. Finally, CD31 staining was performed to visualize cell-to-cell junction of HUVECs cultured in the presence of the different types of the secretome. Specifically, cells were fixed with 4% paraformaldehyde for 5 min. Subsequently, HUVECs were permeabilized with triton 0.1X and blocked with a solution of BSA at the concentration of 1% w/v in PBS for 1 h at 37 °C. The primary antibody against CD31 was added to the cells for 1 h (dilution 1:1000) in 1% BSA. Cells were then washed with PBS and treated with a secondary antibody goat-antimouse tagged with a Alexa Fluor 488 for 1 h. The nuclei of the cells were subsequently stained with DAPI for 5 min. After washing, cells were imaged using a fluorescent microscope.

The Angiogenesis Analyzer in ImageJ was used to determine the number of nodes, number of meshes, the total segment length, number of segments, and number of isolated segments in each image. Results are reported as mean ± deviation standard considering at least 10 images per group.

2.9. Assessment of Anti-inflammatory Properties of the Secretome^{146a} on HUVECs.

HUVECs were seeded in 24-well plates at the cell density of 5×10^4 cells/well and cultured for 24 h using EGM-2 media without any angiogenic growth factor. Then, cells were treated with interleukin-1 (IL-1β) at the concentration of 10 ng/mL to induce an endothelial cell activation similar to the one endothelial cells undergo during early stages of inflammation post-AMI. Three groups were tested in this study: a positive control where HUVECs were left untreated, and two test groups were the media was supplemented with the secretome derived from hASCs nontransfected (secretome), and the one obtained from hASCs transfected with miR-146a (secretome^{146a}). Half of the volume of the media in each well was replaced with secretome for both test groups.

After 4 and 24 h, the mRNA was extracted from the HUVECs using the RNeasy Mini Kit. The total RNA concentration and purity were determined by measuring the optical density at 260 nm. cDNA was synthesized starting from the isolated RNA using the miScript II RT Kit (Qiagen). The qPCR analysis was performed in triplicate for each test group on a Mastercycler Realplex4 (Eppendorf) using predesigned primers and miScript SYBR Green PCR Kit (Qiagen). Fold expression levels of several genes including vascular cellular adhesion molecule-1 (VCAM-1), intracellular adhesion molecule-1 (ICAM-1), tumor necrosis factor receptor-associated factor 6 (TRAF6), and monocyte chemoattractant protein-1 (MCP-1) were evaluated at 4 and 24 h post-treatment. The data were analyzed using the relative ΔΔCt method, and GAPDH was used as the housekeeping gene.

In addition to the gene analysis, the anti-inflammatory effect of the two types of the secretome was investigated by studying the expression of ICAM, and the secretion of MCP-1 by HUVECs treated with IL-1β. HUVECs were washed with PBS three times after 8 h post-treatment with secretome derived from the two different groups. Cells were blocked with 5% w/v goat serum for 15 min, followed by incubation for 30 min with the primary antibody against ICAM (2 μg/mL in 1% goat serum). Cells were then washed three times with PBS and incubated for 30 min with the secondary antibody Anti-Mouse IgG H&L (Alexa Fluor 488) (ab150113) for ICAM-stained samples at the of dilution 1:2000. Cells were washed with PBS three times, recovered using trypsin, resuspended in PBS, and FACs analysis was carried out to quantify the amount of fluorescent positive stained cells in the three different groups using the Attune NxT flow cytometer (Thermo Fischer Scientific).

Finally, HUVECs secretion of MCP-1 was assessed using an ELISA kit for MCP-1 (R&D Systems). A standard curve in the range of 31.3–1000 pg/mL was used to correlate the absorbance values at 450 nm with the amount of protein present in each sample.

3. RESULTS AND DISCUSSION

3.1. Isolation and Characterization of miR-146a-Enriched EVs Derived from hASCs.

The regenerative potential of mesenchymal stem cell (MSC)-derived secretome in promoting the healing and closure of chronic wounds relies on the combination of multiple paracrine molecules secreted by MSCs. These include an array of angiogenic, anti-inflammatory, cardioprotective, and antifibrotic growth factors, cytokines, and EVs.[29,34,35] Specifically, EVs are emerging as key components of the MSC therapeutic paracrine mechanism due to

their ability to carry proangiogenic, anti-inflammatory and antiapoptotic miRNA. Therefore, tailoring their miRNA content represents an ideal approach to increase the therapeutic efficacy of the secretome, leading to a superior regenerative response in the myocardium.

In the present study, hASCs were successfully genetically modified to overexpress miR-146a in the secreted exosomes. We chose to use hASCs over other MSC sources because their minimally invasive isolation technique has low morbidity and produces a high cell yield making this method more clinically feasible than other MSC isolation procedures.[36] In addition, recent studies have shown that hASCs exhibit superior proangiogenic properties when compared to MSCs isolated from bone marrow and Wharton's Jelly.[37] Specifically, hASCs were transfected with a miR-146a oligonucleotide fused to an RNA sequence tag that specifically targets small RNAs into exosomes for packaging (Figure 1). After transfection, the hASCs were cultured for 24 h, and the resulting secretome^{146a} was isolated for characterization and therapeutic assessment. EVs within the hASC-derived secretome were separated to characterize their size, morphology, protein composition, and miRNA content. Electron microscopy images showed that the hASC-EV particles had a bilayer membrane with a primarily uniform circular morphology (Figure 2A,B). NTA analysis revealed that the average diameter of the EVs was 201.2 ± 12.7 nm with 90% of the population having a diameter less than 360.3 nm (range 60–600 nm) (Figure 2C). In addition, the most prevalent subpopulation within the EVs had a diameter of 138.1 nm indicating an exosome-enriched EV population with generally limited size heterogeneity.[38] Western blot of hASCs and hASC-EVs confirmed the presence of transmembrane tetraspanin protein CD63 and the absence of the mitochondrial protein cytochrome c within the hASC-EVs (Figures 2D and S1). These results confirm the endosomal origin of the EVs.[39] Tetraspanins have been shown to bind several integrins and major histocompatibility complex molecules; therefore, the enrichment of CD63 is important for potential protein–protein interactions between EVs and cellular membranes.[24,40] To prove this point, the internalization of EVs into HUVECs was verified by flow cytometry analysis. First, EVs were stained with CD63 and allowed to be internalized by HUVECs for 24 h. A shift in the fluorescence intensity of the HUVECs population was observed, which was indicative of a successful internalization of EVs stained with CD63 (Figure S2).

Finally, the transfection efficiency was confirmed by comparing the miRNA composition of the EVs isolated from secretome (hASCs not transfected) and secretome^{146a} using RT-qPCR, which revealed that EVs from secretome^{146a} were highly enriched with miR-146a ($p < 0.001$) (Figure 2E).

3.2. Angiogenic Properties of the Secretome^{146a}.

An efficient secretome-based therapy aimed to promote wound closure needs to provide the necessary angiogenic cues required to re-establish proper blood perfusion to the damaged tissue. The secretome obtained from nontransfected hASCs displayed a slightly greater amount of angiogenin and VEGF; however, the secretome^{146a} contained larger amounts of several key angiogenic growth factors, including urokinase-type plasminogen activator (uPA), dipeptidyl peptidase IV (DPP IV), endothelin 1, hepatocyte growth factor (HGF), and fibroblast growth factors 1 and 2 (FGF-1 and FGF-2) (Figure 3A). Specifically, uPA

regulates angiogenesis through proteolytic degradation of the extracellular matrix that facilities the subsequent proliferation and migration of endothelial cells.[41,42] FGF-2 has been shown to induce proliferation, promote migration, and inhibit apoptosis of endothelial cells in vitro, in addition, to improve neovascularization in vivo studies.[43–45] Similarly, HGF has been proven to promote endothelial cells proliferation, migration, and tube formation.[46,47] In addition to a greater presence of angiogenic growth factors in the secretome^{146a}, several proangiogenic miRNAs were significantly more expressed in the secretome^{146a} EVs when compared to the EVs in the secretome including, miR-126-3p ($p < 0.01$), miR-210 ($p < 0.01$), miR-143-3p, and miR-130a-3p ($p < 0.05$) (Figure 3B). These specific miRNAs have been shown to increase endothelial cell proliferation and promote neovascularization.[48–50] Finally, the secretome^{146a} EVs also contained significantly less antiangiogenic miRNA compared to the secretome including, miR-26a-5p ($p < 0.05$), miR-92a-3p ($p < 0.05$), miR-15-5p ($p < 0.01$), and miR-222-3p ($p < 0.05$) (Figure 3C).[51,52]

The angiogenic efficacy of the two groups was assessed using three different in vitro HUVEC assays. HUVECs cultured in endothelial growth media without the addition of VEGF and FGF-B were used as the control group (Ctrl (−)). Angiogenesis is a tightly regulated multistep physiological process that begins with the migration and proliferation of activated endothelial cells through the perivascular tissue to form capillary sprouts originating from existing vessels.[17] Therefore, an MTS assay was used to determine the effect each secretome type had on HUVECs proliferation. After 24 h, a higher cell number was observed in the secretome^{146a} group when compared to the control and the secretome group ($p < 0.05$) (Figure 4B). Next, the ability of the secretome to promote HUVEC migration was determined using silicone inserts that allowed the formation of a defined cell-free gap of 1 mm in the center of a confluent HUVEC monolayer. After 6 h minimal migration had occurred in all three groups; however, at 24 h, the HUVECs treated with the secretome^{146a} had migrated to cover 55% of the cell-free area as opposed to the HUVECs in the Ctrl (−) and secretome groups, which only covered 27 and 37%, respectively ($p < 0.001$ and $p < 0.05$, respectively; Figure 4A and C).

After the formation of the capillary sprouts, it is necessary for endothelial cells to properly align and form tubes with a patent lumen that can provide the scaffold needed for the basement membrane deposition.[53] The capacity of the secretome to induce the formation of tub-like structures by HUVECs was evaluated using a Matrigel assay. HUVECs were cultured on Matrigel-coated wells either in the presence of the secretome or secretome^{146a} for 16 h before images were taken (Figures 5A and S3). Similar to the proliferation and migration assay, the secretome^{146a} caused the formation of significantly greater number of nodes ($p < 0.01$; Figure 5B), complete tubes ($p < 0.01$; Figure 5C), and segments ($p < 0.001$; Figure 5D) as well as longer segment lengths ($p < 0.001$; Figure 5E). Additionally, a reduction in the number of isolated segments ($p < 0.001$; Figure 5F) was also observed in the secretome^{146a} group compared to the secretome group. Similar trends were seen when comparing the secretome^{146a} to the Ctrl (−) group ($p < 0.001$; Figure 5B–F). However, no significant difference was observed in the presence of CD31 between the groups tested with the different types of the secretome (Figure S4). Overall, these assays together confirmed the superior angiogenic efficacy of the secretome^{146a}. Therefore, based on these results and the composition analysis, the transfection of hASCs with miR-146a resulted in the production of

a secretome with superior proangiogenic efficacy compared to the one isolated from nontransfected hASCs. These results are in agreement with a previous study that correlated the improvement in angiogenesis at the wound site after an acute myocardial infarction to the treatment with exosomes that contained an abundant presence of miR-146a.[32]

3.3. Immunomodulatory Properties of the Secretome^{146a}.

After an injury occurs, an acute inflammatory response is needed for proper clearance of damaged and necrotic tissue and to prevent infection. However, the intensity and duration of this inflammatory response must be tightly regulated to prevent further damage to the tissue. Therefore, an efficient secretome-based therapy should also be able to modulate the inflammatory response to promote effective wound healing.[54]

We compared the cytokine and miRNA composition of the two different types of the secretome to identify paracrine molecules that could potentially modulate an inflammatory response. The comparison of the inflammatory cytokine composition of each secretome indicated that only one cytokine, granulocyte colony-stimulating factor, was expressed exclusively in the secretome^{146a} (Figure 6A). Despite the fact that G-SCF has not been shown to have anti-inflammatory properties, its known ability to recruit stem/progenitor cells inhibits apoptosis and promote angiogenesis in the context of the tissue regeneration could support any enhanced therapeutic efficacy observed with secretome^{146a} treatment.[55,56] The remaining cytokines, including CCL-1, CCL-2, TRAP, and IL-4, were detected at comparable levels in the two different secretomes. Furthermore, the miRNA present in the EVs originating from the two different secretomes was compared and showed that several antiapoptotic miRNAs were significantly upregulated in the secretome^{146a} (miR-22-3p ($p < 0.05$), miR-214-5p ($p < 0.05$), miR-24-3p ($p < 0.01$)) in addition to, a significant downregulation in multiple proapoptotic miRNAs (miR-29b-3p ($p < 0.05$), let-7c ($p < 0.01$), and let-7b-5p ($p < 0.05$)) (Figure 6B,C).[57–60] Therefore, the miRNA in the secretome,^{146a} EVs represent an ideal treatment for the inhibition of inflammation within the myocardium due to the fact that the damage-associated molecular patterns released by apoptotic and necrotic cells are key regulators in the activation of endothelial cells to an inflammatory state.

A key target of the inflammatory process within the damaged myocardium is the endothelium, which directly controls the extravasation of leukocytes that are recruited to the infarct area from the spleen.[61] Precisely, in the initial stages of inflammation, upregulation of leukocyte adhesion molecules (VCAM, ICAM, E-selectin) on endothelial cells is vital for efficient capture of neutrophils and subsequent mediation of their tethering and rolling process along the venular endothelium.[61] To mimic the process of endothelial cells inflammatory activation by circulating cytokines, we exposed HUVECs to the proinflammatory cytokine, IL-1β, and assessed the ability of the secretome to modulate the subsequent HUVEC inflammatory activation.

The anti-inflammatory efficacy of the secretome and secretome^{146a} was then assessed evaluating the gene expression of several genes involved in the regulation of the inflammatory response in HUVECs. First, IL-1β was shown to cause upregulation in the gene expression of *ICAM*, *MCP-1*, and *VCAM*, and no difference in gene expression

between all three test groups was observed 4 h after treatment (Figure 7A). However, 24 h after treatment, the secretome^{146a} was shown to significantly decrease the gene expression of *ICAM* ($p < 0.01$), *MCP-1* ($p < 0.01$), and *VCAM* ($p < 0.05$) compared to the secretome-treated group (Figure 7B).

In addition to the gene upregulation of adhesion molecules for leukocytes, activated endothelial cells also serve as an important source of cytokines and chemokines within the damaged tissue.[61,62] Therefore, we also studied the effect the two different types of the secretome had on MCP-1 secretion by IL-1β-activated endothelial cells. Secretome^{146a} was also able to significantly suppress the secretion of MCP-1 by HUVECs after IL-1β treatment compared to the Ctrl (−) and secretome group ($p < 0.001$ and $p < 0.05$, respectively; Figure 7C). The expression of adhesion protein ICAM was also shown to decrease upon secretome treatment with the secretome^{146a} group, which exhibited the lowest expression among the three test groups (Figure 7D).

Together these results demonstrate that secretome^{146a} has the capacity to modulate several of the inflammatory responses exhibited by endothelial cells upon activation by inflammatory cytokines such as IL-1β. Additionally, these results confirm that the secretome retrieved from transfected hASCs has superior anti-inflammatory properties and could potentially be used in the late-stage resolution of the acute inflammation at the wound site to downregulate endothelial cell activation and, therefore, inhibit excessive transmigration of neutrophils.

4. CONCLUSIONS

In this study, we have successfully enhanced the therapeutic efficacy of hASC-derived secretome by transfecting hASC with miR-146a. By using this specific miRNA sequence-tagged oligonucleotide, we efficiently caused the EVs secreted by hASC to be enriched with the known therapeutic miRNA. The resulting EV population exhibited a size and protein composition indicative of an exosome-enriched population, a subpopulation of EVs that have been implicated in the tissue regeneration and wound healing. Within the EVs secreted by the transfected hASCs, we detected an increased concentration of proangiogenic and antiapoptotic miRNAs as well as a decreased concentration of antiangiogenic and proapoptotic miRNAs when we compared them to the EVs secreted by nontransfected hASCs. Furthermore, the growth factor and cytokine composition of this secretome showed a significantly higher concentration of several key proangiogenic, chemotactic, and antiapoptotic proteins, which are shown to promote wound healing and tissue regeneration. The enhanced composition of therapeutic paracrine molecules observed in the secretome^{146a} also corresponded to a superior therapeutic efficacy in vitro. Specifically, the secretome^{146a} was shown to significantly upregulate the proliferation, migration, and tube formation of endothelial cells proving enhanced proangiogenic properties. Additionally, the secretome^{146a} was able to suppress the proinflammatory behavior of IL-1β-activated endothelial cells by reducing the expression of leukocyte adhesion molecules and the secretion of proinflammatory cytokines. Overall, these results suggest that the secretome^{146a} represents a viable treatment option for the promotion of angiogenesis and modulation of the inflammation and, therefore, could potentially be used to promote the healing of chronic

wounds. To further investigate the therapeutic efficacy of the secretome^{146a}, future in vivo studies using diabetic or burn chronic wound models could be used to specifically assess whether the proangiogenic and anti-inflammatory properties support tissue repair and regeneration.

Supplementary Material

Refer to Web version on PubMed Central for supplementary material.

ACKNOWLEDGMENTS

R.W. acknowledges the financial support from NIH-Biotechnology Predoctoral Research Training Program (T32-GM008359). A.P. acknowledges an investigator grant provided by the Institutional Development Award (IDeA) from the National Institute of General Medical Sciences (NIGMS) of the NIH Award Number P20GM103638 and Umbilical Cord Matrix Project fund from State of Kansas.

REFERENCES

(1). Badiavas EV; Falanga V Treatment of chronic wounds with bone marrow–derived cells. Arch. Dermatol 2003, 139, 510–516. [PubMed: 12707099]

(2). Falanga V; Iwamoto S; Chartier M; Yufit T; Butmarc J; Kouttab N; Shrayer D; Carson P Autologous bone marrow–derived cultured mesenchymal stem cells delivered in a fibrin spray accelerate healing in murine and human cutaneous wounds. Tissue Eng. 2007, 13, 1299–1312. [PubMed: 17518741]

(3). Wu Y; Chen L; Scott PG; Tredget EE Mesenchymal stem cells enhance wound healing through differentiation and angiogenesis. Stem Cells 2007, 25, 2648–2659. [PubMed: 17615264]

(4). Braunwald E Cell-Based Therapy in Cardiac Regeneration: An Overview. Circ. Res 2018, 123, 132–137. [PubMed: 29976683]

(5). Cerqueira MT; Pirraco RP; Marques AP Stem cells in skin wound healing: are we there yet? Adv. Wound Care 2016, 5, 164–175.

(6). Chen L; Xu Y; Zhao J; Zhang Z; Yang R; Xie J; Liu X; Qi S Conditioned medium from hypoxic bone marrow-derived mesenchymal stem cells enhances wound healing in mice. PLoS One 2014, 9, No. e96161. [PubMed: 24781370]

(7). Lee EY; Xia Y; Kim WS; Kim MH; Kim TH; Kim KJ; Park BS; Sung JH Hypoxia-enhanced wound-healing function of adipose-derived stem cells: Increase in stem cell proliferation and up-regulation of VEGF and bFGF. Wound Repair Regener. 2009, 17, 540–547.

(8). Jun E; Zhang Q; Yoon B; Moon J-H; Lee G; Park G; Kang P; Lee J; Kim A; You S Hypoxic conditioned medium from human amniotic fluid-derived mesenchymal stem cells accelerates skin wound healing through TGF-β/SMAD2 and PI3K/Akt pathways. Int. J. Mol. Sci 2014, 15, 605–628. [PubMed: 24398984]

(9). Lee SM; Lee SC; Kim S-J Contribution of human adipose tissue-derived stem cells and the secretome to the skin allograft survival in mice. J. Surg. Res 2014, 188, 280–289. [PubMed: 24560349]

(10). Sun D; Gill B; Babbar P; Kuang M; Lin D; Damaser M PD09-03 Mesenchymal stem cell-derived exosomes contribute to secretome-mediated renal recovery after ischemic injury in rats. J. Urol 2019, 201, No. e154.

(11). Robert AW; Azevedo Gomes F; Rode MP; Marques da Silva M; Veleirinho MBR; Maraschin M; Hayashi L; Wosgrau Calloni G; Stimamiglio MA The skin regeneration potential of a pro-angiogenic secretome from human skin-derived multipotent stromal cells. J. Tissue Eng 2019, 10, No. 2041731419833391.

(12). Hacker S; Mittermayr R; Nickl S; Haider T; Lebherz-Eichinger D; Beer L; Mitterbauer A; Leiss H; Zimmermann M; Schweiger T; et al. Paracrine factors from irradiated peripheral blood

mononuclear cells improve skin regeneration and angiogenesis in a porcine burn model. Sci. Rep 2016, 6, No. 25168. [PubMed: 27125302]

(13). Wagner T; Traxler D; Simader E; Beer L; Narzt M-S; Gruber F; Madlener S; Laggner M; Erb M; Vorstandlechner V; et al. Different pro-angiogenic potential of γ-irradiated PBMC-derived secretome and its subfractions. Sci. Rep 2018, 8, No. 18016. [PubMed: 30573762]

(14). Waters R; Alam P; Pacelli S; Chakravarti AR; Ahmed RP; Paul A Stem cell-inspired secretome-rich injectable hydrogel to repair injured cardiac tissue. Acta Biomater. 2017, 69, 95–106. [PubMed: 29281806]

(15). Waters R; Pacelli S; Maloney R; Medhi I; Ahmed RP; Paul A Stem cell secretome-rich nanoclay hydrogel: a dual action therapy for cardiovascular regeneration. Nanoscale 2016, 8, 7371–7376. [PubMed: 26876936]

(16). Boon RA; Dimmeler S MicroRNAs in myocardial infarction. Nat. Rev. Cardiol 2015, 12, No. 135. [PubMed: 25511085]

(17). Awada HK; Hwang MP; Wang Y Towards comprehensive cardiac repair and regeneration after myocardial infarction: Aspects to consider and proteins to deliver. Biomaterials 2016, 82, 94–112. [PubMed: 26757257]

(18). Lu M; Xing H; Yang Z; Sun Y; Yang T; Zhao X; Cai C; Wang D; Ding P Recent advances on extracellular vesicles in therapeutic delivery: Challenges, solutions, and opportunities. Eur. J. Pharm. Biopharm 2017, 119, 381–395. [PubMed: 28739288]

(19). Maring JA; Lodder K; Mol E; Verhage V; Wiesmeijer KC; Dingenouts CK; Moerkamp AT; Deddens JC; Vader P; Smits AM; et al. Cardiac Progenitor Cell-Derived Extracellular Vesicles Reduce Infarct Size and Associate with Increased Cardiovascular Cell Proliferation. J. Cardiovasc. Transl. Res 2019, 12, 5–17. [PubMed: 30456736]

(20). Lopatina T; Favaro E; Grange C; Cedrino M; Ranghino A ; Occhipinti S; Fallo S; Buffolo F; Gaykalova DA; Zanone MM; et al. PDGF enhances the protective effect of adipose stem cell-derived extracellular vesicles in a model of acute hindlimb ischemia. Sci. Rep 2018, 8, No. 17458. [PubMed: 30514962]

(21). Luan X; Sansanaphongpricha K; Myers I; Chen H; Yuan H; Sun D Engineering exosomes as refined biological nanoplatforms for drug delivery. Acta Pharmacol. Sin 2017, 38, No. 754. [PubMed: 28392567]

(22). Cha JM; Shin EK; Sung JH; Moon GJ; Kim EH; Cho YH; Dal Park H; Bae H; Kim J; Bang OY Efficient scalable production of therapeutic microvesicles derived from human mesenchymal stem cells. Sci. Rep 2018, 8, No. 1171.

(23). Valadi H; Ekström K; Bossios A; Sjöstrand M; Lee JJ; Lötvall JO Exosome-mediated transfer of mRNAs and microRNAs is a novel mechanism of genetic exchange between cells. Nat. Cell Biol 2007, 9, No. 654. [PubMed: 17486113]

(24). Armstrong JP; Holme MN; Stevens MM Re-engineering extracellular vesicles as smart nanoscale therapeutics. ACS Nano 2017, 11, 69–83. [PubMed: 28068069]

(25). Sahoo S; Losordo DW Exosomes and cardiac repair after myocardial infarction. Circ. Res 2014, 114, 333–344. [PubMed: 24436429]

(26). Seeger FH; Zeiher AM; Dimmeler S MicroRNAs in stem cell function and regenerative therapy of the heart. Arterioscler., Thromb., Vasc. Biol 2013, 33, 1739–1746. [PubMed: 23864723]

(27). Van der Pol E; Böing AN; Harrison P; Sturk A; Nieuwland R Classification, functions, and clinical relevance of extracellular vesicles. Pharmacol. Rev 2012, 64, 676–705. [PubMed: 22722893]

(28). Rani S; Ryan AE; Griffin MD; Ritter T Mesenchymal stem cell-derived extracellular vesicles: toward cell-free therapeutic applications. Mol. Ther 2015, 23, 812–823. [PubMed: 25868399]

(29). Rani S; Ritter T The Exosome-A Naturally Secreted Nanoparticle and its Application to Wound Healing. Adv. Mater 2016, 28, 5542–5552. [PubMed: 26678528]

(30). Xu J; Wu W; Zhang L; Dorset-Martin W; Morris MW; Mitchell ME; Liechty KW The role of microRNA-146a in the pathogenesis of the diabetic wound-healing impairment: correction with mesenchymal stem cell treatment. Diabetes 2012, 61, 2906–2912. [PubMed: 22851573]

(31). Cheng HS; Sivachandran N; Lau A; Boudreau E; Zhao JL ; Baltimore D; Delgado-Olguin P; Cybulsky MI; Fish JE MicroRNA-146 represses endothelial activation by inhibiting proinflammatory pathways. EMBO Mol. Med 2013, 5, 1017–1034. [PubMed: 23733368]

(32). Ibrahim AG-E; Cheng K; Marbán E Exosomes as critical agents of cardiac regeneration triggered by cell therapy. Stem Cell Rep. 2014, 2, 606–619.

(33). Huang W; Tian S-S; Hang P-Z; Sun C; Guo J; Du Z-M Combination of microRNA-21 and microRNA-146a attenuates cardiac dysfunction and apoptosis during acute myocardial infarction in mice. Mol. Ther.-Nucleic Acids 2016, 5, No. e296. [PubMed: 26978580]

(34). Demidova-Rice TN; Hamblin MR; Herman IM Acute and impaired wound healing: pathophysiology and current methods for drug delivery, part 2: role of growth factors in normal and pathological wound healing: therapeutic potential and methods of delivery. Adv. Skin Wound Care 2012, 25, No. 349. [PubMed: 22820962]

(35). Ranganath SH; Levy O; Inamdar MS; Karp JM Harnessing the mesenchymal stem cell secretome for the treatment of cardiovascular disease. Cell Stem Cell 2012, 10, 244–258. [PubMed: 22385653]

(36). Li T-S; Cheng K; Malliaras K; Smith RR; Zhang Y; Sun B ; Matsushita N; Blusztajn A; Terrovitis J; Kusuoka H Direct comparison of different stem cell types and subpopulations reveals superior paracrine potency and myocardial repair efficacy with cardiosphere-derived cells. J. Am. Coll. Cardiol 2012, 59, 942–953. [PubMed: 22381431]

(37). Amable PR; Teixeira MVT; Carias RBV; Granjeiro JM; Borojevic R Protein synthesis and secretion in human mesenchymal cells derived from bone marrow, adipose tissue and Wharton's jelly. Stem Cell Res. Ther 2014, 5, No. 53. [PubMed: 24739658]

(38). Vizoso F; Eiro N; Cid S; Schneider J; Perez-Fernandez R Mesenchymal stem cell secretome: toward cell-free therapeutic strategies in regenerative medicine. Int. J. Mol. Sci 2017, 18, No. 1852.

(39). Lötvall J; Hill AF; Hochberg F; Buzás EI; Di Vizio D; Gardiner C; Gho YS; Kurochkin IV; Mathivanan S; Quesenberry P Minimal Experimental Requirements for Definition of Extracellular Vesicles and their Functions: A Position Statement from the International Society for Extracellular Vesicles; Taylor & Francis, 2014.

(40). Koppers-Lalic D; Hogenboom MM; Middeldorp JM; Pegtel DM Virus-modified exosomes for targeted RNA delivery; a new approach in nanomedicine. Adv. Drug Delivery Rev 2013, 65, 348–356.

(41). Stepanova V; Jayaraman PS; Zaitsev SV; Lebedeva T; Bdeir K; Kershaw R; Holman KR; Parfyonova YV; Semina EV; Beloglazova IB; Tkachuk VA; Cines DB Urokinase-type Plasminogen Activator (uPA) Promotes Angiogenesis by Attenuating Proline-rich Homeodomain Protein (PRH) Transcription Factor Activity and De-repressing Vascular Endothelial Growth Factor (VEGF) Receptor Expression. J. Biol. Chem 2016, 291, 15029–15045. [PubMed: 27151212]

(42). Montuori N; Ragno P Role of uPA/uPAR in the modulation of angiogenesis. Chem. Immunol. Allergy 2013, 99, 105–122. [PubMed: 24217605]

(43). Shi H-X; Lin C; Lin B-B; Wang Z-G; Zhang H-Y; Wu F-Z; Cheng Y; Xiang L-J; Guo D-J; Luo X; et al. The anti-scar effects of basic fibroblast growth factor on the wound repair in vitro and in vivo. PLoS One 2013, 8, No. e59966. [PubMed: 23565178]

(44). Losi P; Briganti E; Errico C; Lisella A; Sanguinetti E; Chiellini F; Soldani G Fibrin-based scaffold incorporating VEGF- and bFGF-loaded nanoparticles stimulates wound healing in diabetic mice. Acta Biomater. 2013, 9, 7814–7821. [PubMed: 23603001]

(45). Wu J; Ye J; Zhu J; Xiao Z; He C; Shi H; Wang Y; Lin C ; Zhang H; Zhao Y Heparin-based coacervate of FGF2 improves dermal regeneration by asserting a synergistic role with cell proliferation and endogenous facilitated VEGF for cutaneous wound healing. Biomacromolecules 2016, 17, 2168–2177. [PubMed: 27196997]

(46). Awada H; Johnson N; Wang Y Dual Delivery of Vascular Endothelial Growth Factor and Hepatocyte Growth Factor Coacervate Displays Strong Angiogenic Effects. Macromol. Biosci 2014, 14, 679–686. [PubMed: 24452960]

(47). Ruvinov E; Leor J; Cohen S The effects of controlled HGF delivery from an affinity-binding alginate biomaterial on angiogenesis and blood perfusion in a hindlimb ischemia model. Biomaterials 2010, 31, 4573–4582. [PubMed: 20206988]

(48). Arif M; Pandey R; Alam P; Jiang S; Sadayappan S; Paul A; Ahmed RPH MicroRNA-210-mediated proliferation, survival, and angiogenesis promote cardiac repair post myocardial infarction in rodents. J. Mol. Med 2017, 95, 1369–1385. [PubMed: 28948298]

(49). Schober A; Nazari-Jahantigh M; Wei Y; Bidzhekov K; Gremse F; Grommes J; Megens RT; Heyll K; Noels H; Hristov M MicroRNA-126-5p promotes endothelial proliferation and limits atherosclerosis by suppressing Dlk1. Nat. Med 2014, 20, No. 368. [PubMed: 24584117]

(50). Jakob P; Doerries C; Briand S; Mocharla P; Kränkel N; Besler C; Mueller M; Manes C; Templin C; Baltes C; et al. Loss of angiomiR-126 and 130a in angiogenic early outgrowth cells from patients with chronic heart failure: role for impaired in vivo neovascularization and cardiac repair capacity. Circulation 2012, 112, No. 093906.

(51). Lucas T; Bonauer A; Dimmeler S RNA therapeutics in cardiovascular disease. Crc. Res 2018, 123, 205–220.

(52). Gimona M; Pachler K; Laner-Plamberger S; Schallmoser K; Rohde E Manufacturing of human extracellular vesicle-based therapeutics for clinical use. Int. J. Mol. Sci 2017, 18, No. 1190.

(53). Guidolin D; Albertin G; Ribatti D Exploring in vitro angiogenesis by image analysis and mathematical modeling. Microscopy 2010, 2, 876–884.

(54). Eming SA; Krieg T; Davidson JM Inflammation in wound repair: molecular and cellular mechanisms. J. Invest. Dermatol 2007, 127, 514–525. [PubMed: 17299434]

(55). Harada M; Qin Y; Takano H; Minamino T; Zou Y; Toko H; Ohtsuka M; Matsuura K; Sano M; Nishi J.-i. G-CSF prevents cardiac remodeling after myocardial infarction by activating the Jak-Stat pathway in cardiomyocytes. Nat. Med 2005, 11, No. 305. [PubMed: 15723072]

(56). Srinivas G; Anversa P; Frishman WH Cytokines and myocardial regeneration: a novel treatment option for acute myocardial infarction. Cardiol. Rev 2009, 17, 1–9. [PubMed: 19092364]

(57). Tong Z; Jiang B; Wu Y; Liu Y; Li Y; Gao M; Jiang Y; Lv Q; Xiao X MiR-21 protected cardiomyocytes against doxorubicin-induced apoptosis by targeting BTG2. Int. J. Mol. Sci 2015, 16, 14511–14525. [PubMed: 26132560]

(58). Huang Z; Wu S; Kong F; Cai X; Ye B; Shan P; Huang W Micro RNA-21 protects against cardiac hypoxia/reoxygenation injury by inhibiting excessive autophagy in H9c2 cells via the Akt/mTOR pathway. J. Cell. Mol. Med 2017, 21, 467–474. [PubMed: 27680680]

(59). Xiao X; Lu Z; Lin V; May A; Shaw DH; Wang Z; Che B; Tran K; Du H; Shaw PX MicroRNA miR-24-3p Reduces Apoptosis and Regulates Keap1-Nrf2 Pathway in Mouse Cardiomyocytes Responding to Ischemia/Reperfusion Injury. Oxid. Med. Cell. Longevity 2018, 2018, No. 7042105.

(60). Seeger T; Xu Q-F; Muhly-Reinholz M; Fischer A; Kremp E-M; Zeiher AM; Dimmeler S Inhibition of let-7 augments the recruitment of epicardial cells and improves cardiac function after myocardial infarction. J. Mol. Cell. Cardiol 2016, 94, 145–152. [PubMed: 27071338]

(61). Prabhu SD; Frangogiannis NG The biological basis for cardiac repair after myocardial infarction: from inflammation to fibrosis. Circ. Res 2016, 119, 91–112. [PubMed: 27340270]

(62). Frangogiannis NG; Mendoza LH; Lewallen M; Michael LH; Smith CW; Entman ML Induction and suppression of interferon-inducible protein 10 in reperfused myocardial infarcts may regulate angiogenesis. FASEB J. 2001, 15, 1428–1430. [PubMed: 11387246]

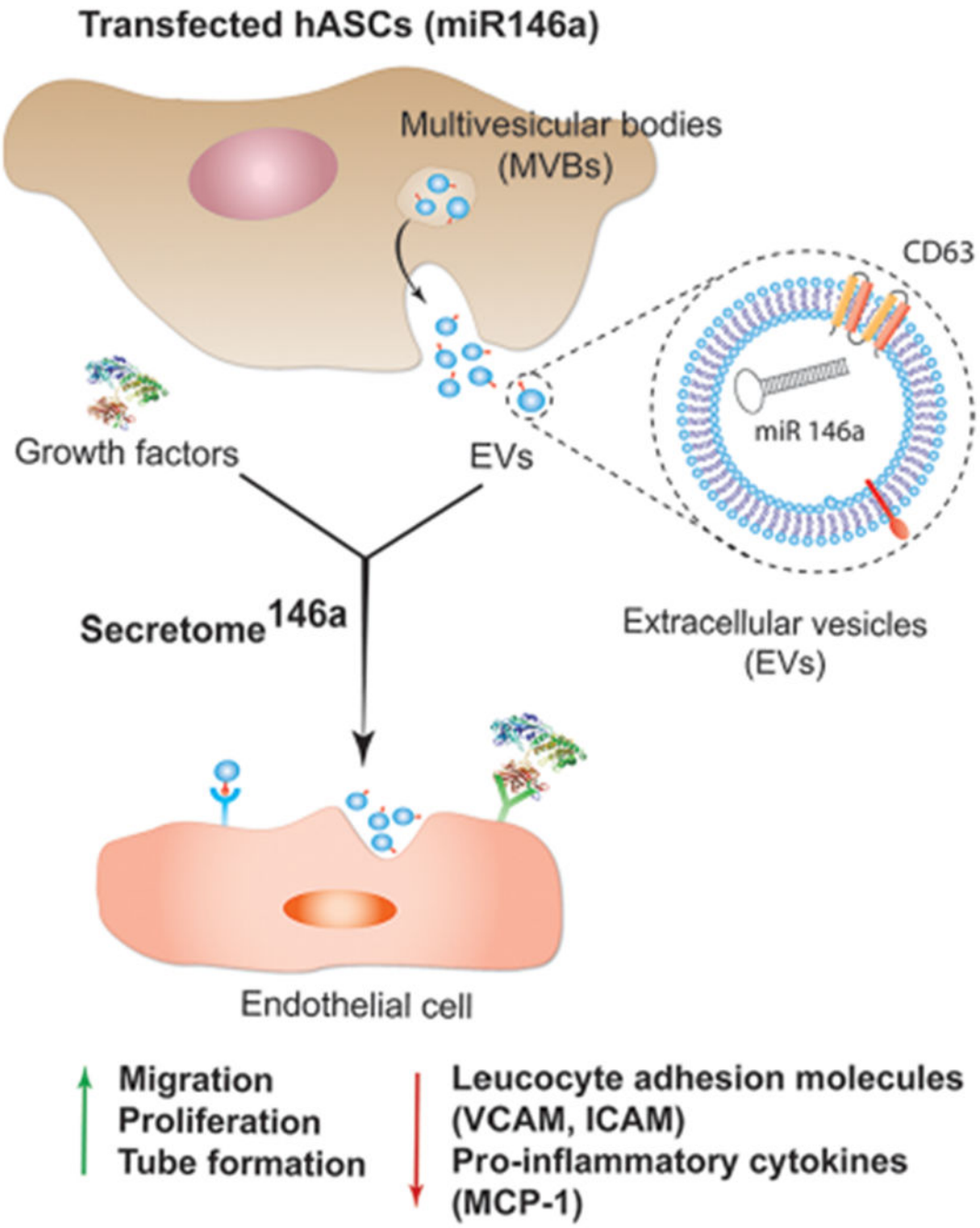

Figure 1.

Schematic representing the process of hASCs transfection with miR-146a. Upon transfection, hASCs start secreting enriched extracellular vesicles containing miR-146a. The enriched secretome will possess a proangiogenic and anti-inflammatory effect on endothelial cells due to the presence of the miR-146a carried in the exosome subpopulation of EVs. Abbreviations: human adipose-derived stem cells (hASCs), multivesicular body (MVB), vascular cell adhesion protein (VCAM), intercellular adhesion molecule (ICAM), and monocyte chemoattractant protein-1 (MCP-1).

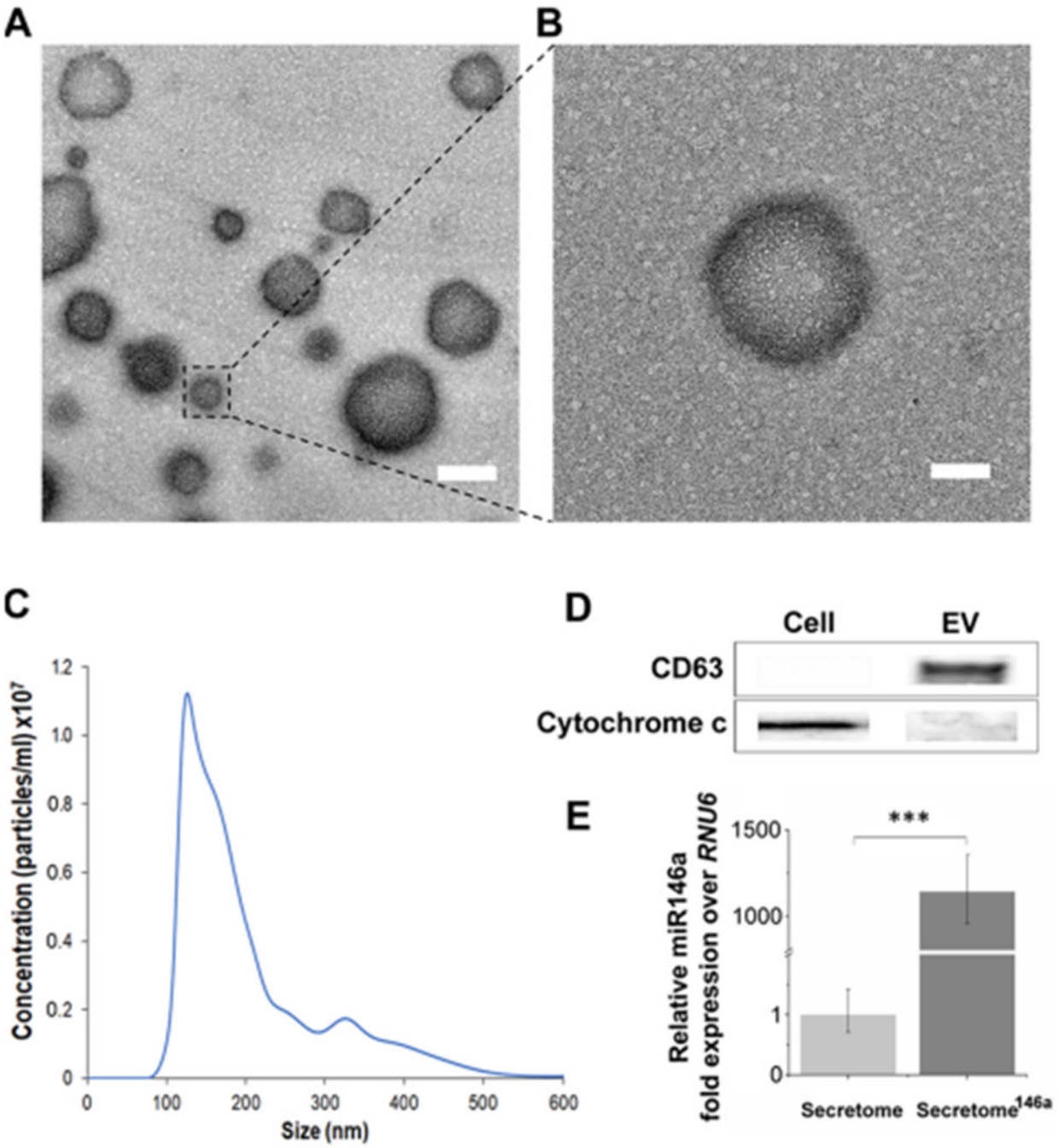

Figure 2.

Characterization of EVs derived from transfected hASCs. (A) TEM images of the extracellular vesicles secreted by hASCs. Scale bar = 200 nm. (B) Corresponding higher magnification where it is evident the presence of the double bilayer of the exosomes. Scale bar = 100 nm. (C) Representative size distribution curve obtained by the NTA analysis of the extracellular vesicle population secreted by hASCs. It is evident a bimodal distribution with the larger population displaying a smaller size in the range of 150–200 nm. (D) Western blot analysis was carried out to test the presence of specific protein markers in the exosome

population compared to the whole cell lysate. (E) Relative fold expression of miR-146a in the exosomes obtained from the transfected hASCs. Results are normalized based on the level expression in the control group using *RNU6* as the housekeeping gene.

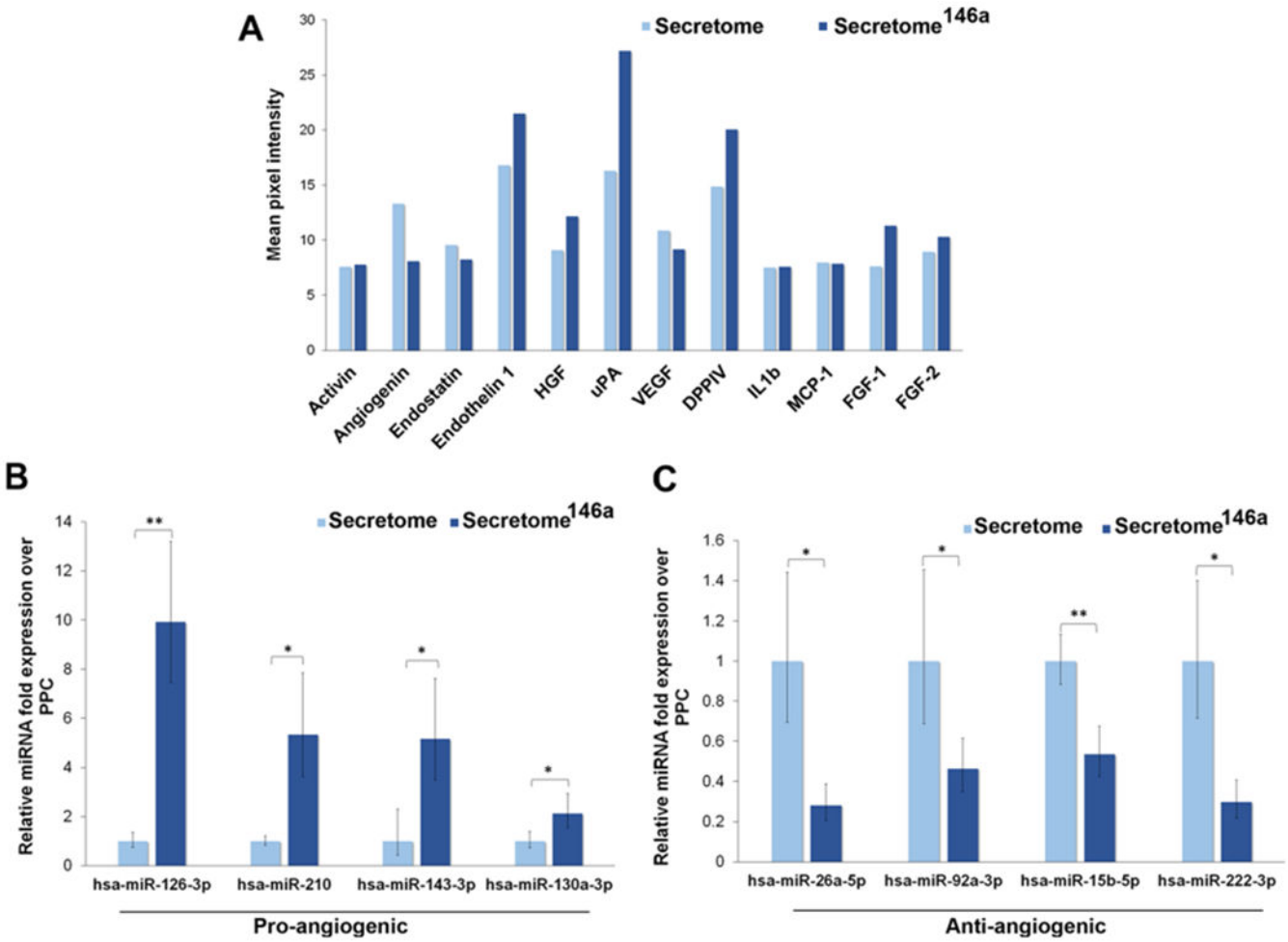

Figure 3.

Comparison of the growth factor composition and miRNA composition of the secretome derived from transfected vs nontransfected hASCs with miR-146a. The group named secretome^{146a} refers to hASCs transfected with the miR-146a. (A) Angiogenic array analysis displaying the difference in the secreted amount of several angiogenic growth factors. (B) qPCR analysis of the main proangiogenic miRNA found in the EVs of the two types of the secretome. (C) qPCR analysis of the main antiangiogenic miRNA found in the EVs of the two types of the secretome.

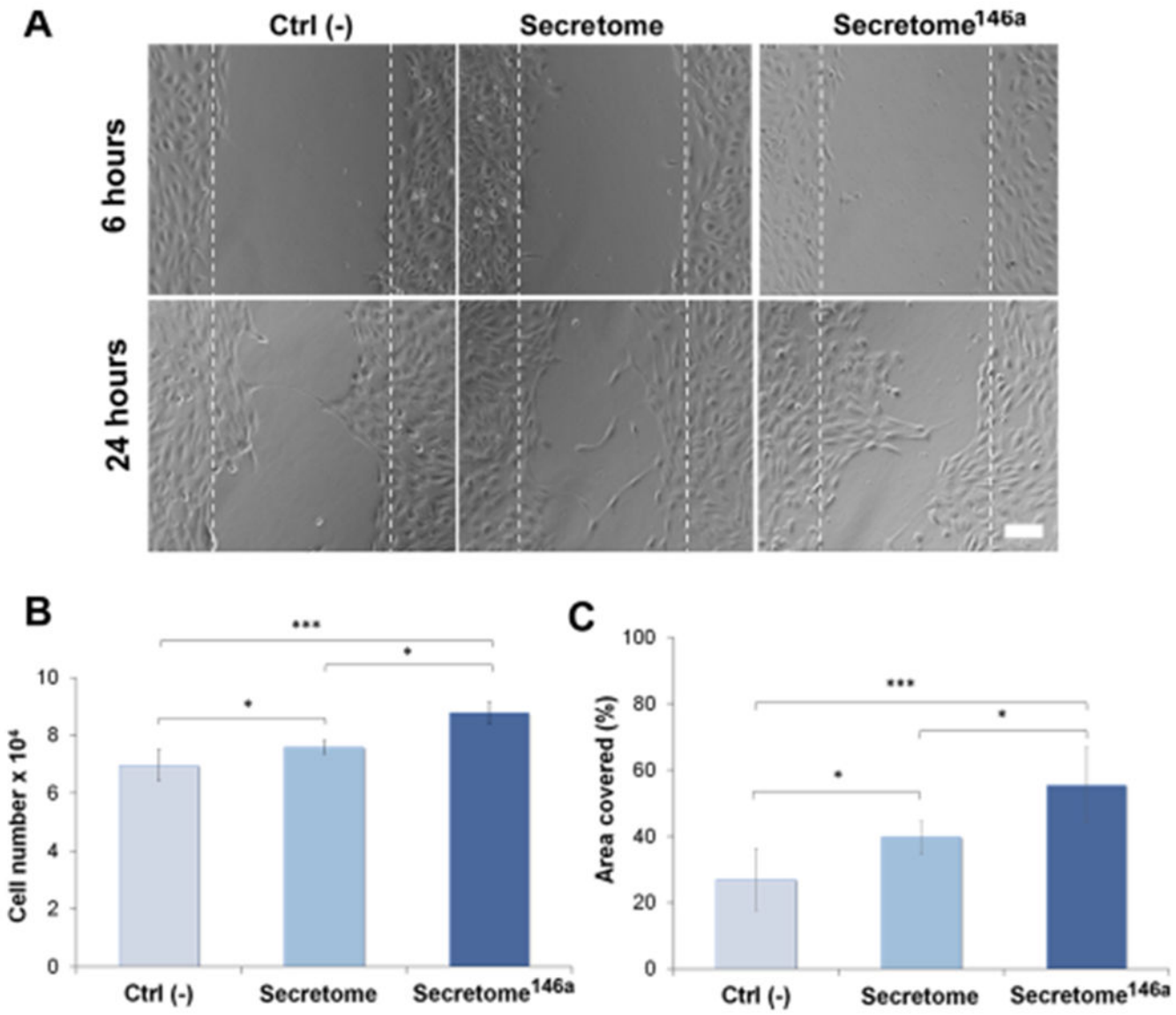

Figure 4.

Evaluation of the angiogenic properties of the two different types of the secretome. (A) Representative bright-field images of the scratch assay carried out at 6 and 24 h for the free different groups. The dotted white lines define the original area of the scratch. Scale bar = 200 μm. (B) HUVEC cell proliferation monitored after 24 h using an MTS assay ($n = 5$). Cells were treated with different types of the secretome and compared to the cells cultured without the addition of any angiogenic growth factor (Ctrl (−)). (C) Corresponding quantification of the area covered by the HUVECs over 24 h of migration. ImageJ analysis was used to quantify the percentage of area covered ($n = 10$). Results are reported as mean ± deviation standard. *$p < 0.05$, **$p < 0.01$ ***$p < 0.001$.

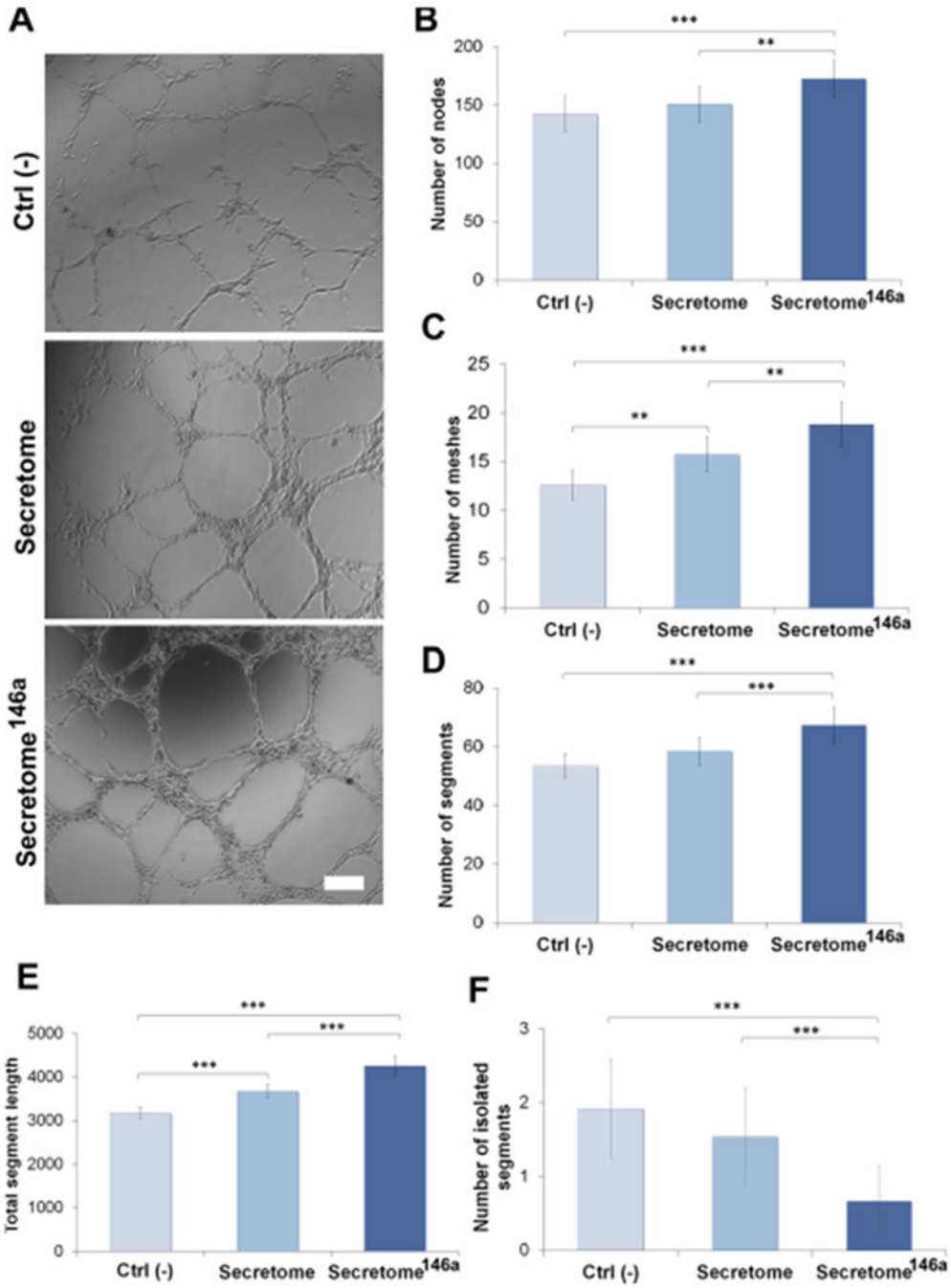

Figure 5.

Tube formation assay of HUVEC to test the proangiogenic properties of the secretome. (A) Bright-field images of HUVECs cultured on Matrigel and treated with different types of the secretome. The negative control group (Ctrl (−)) was represented by endothelial cells cultured without any angiogenic growth factor. Scale bar = 200 μm. ImageJ quantification of several parameters regarding the network structure including (B) number of nodes (C) number of meshes (D) number of segments (E) total segments length in the network, and (F)

number of isolated segments. The results are reported as mean ± deviation standard ($n = 10$). *$p < 0.05$, **$p < 0.01$ ***$p < 0.001$.

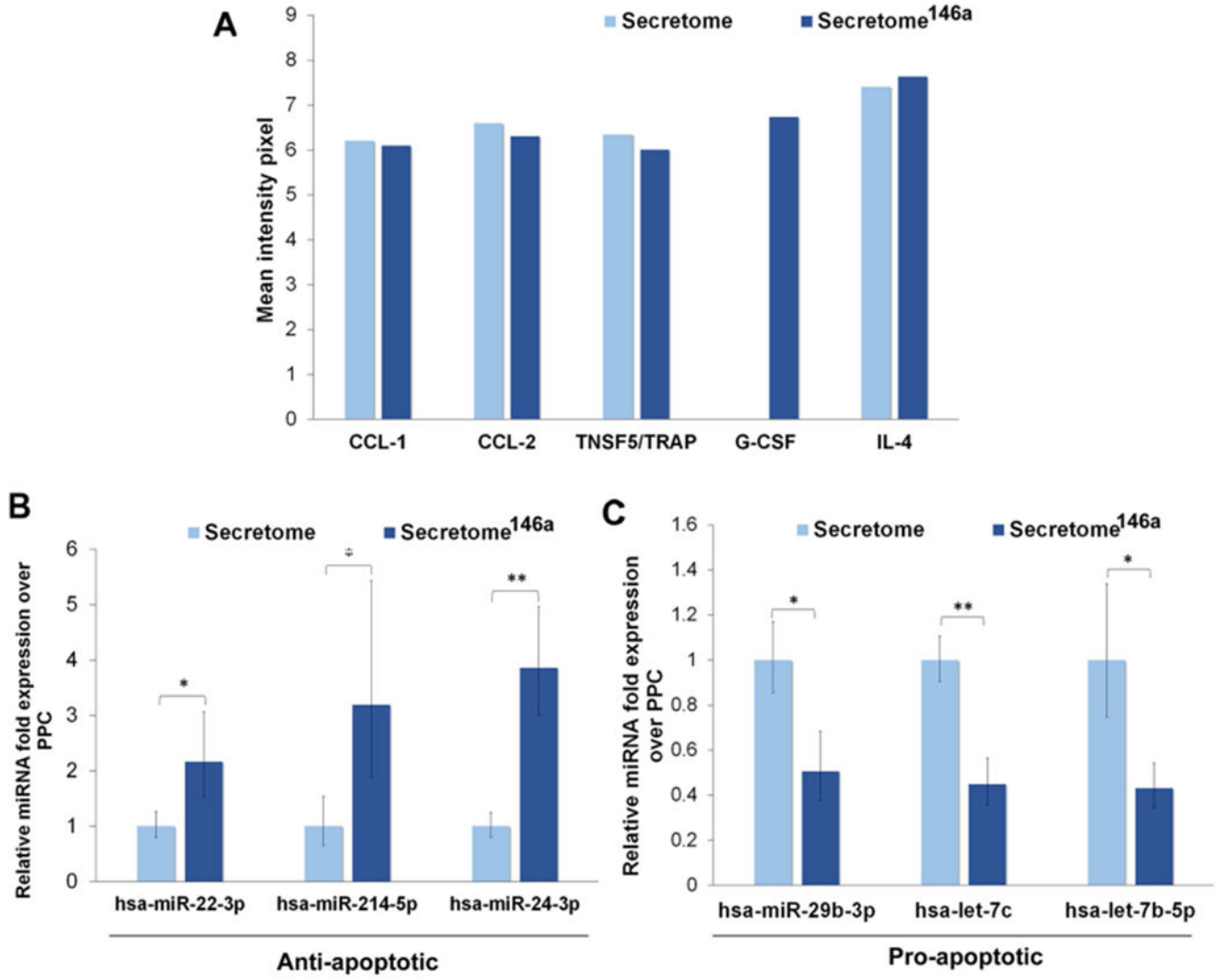

Figure 6.

Characterization of the cytokines and miRNA composition. (A) Cytokine array results of the different types of cytokines found in the two different types of the secretome. (B) Antiapoptotic miRNA found in the EVs of the two types of the secretome. (C) Proapoptotic miRNA found in the EVs of the two types of the secretome.

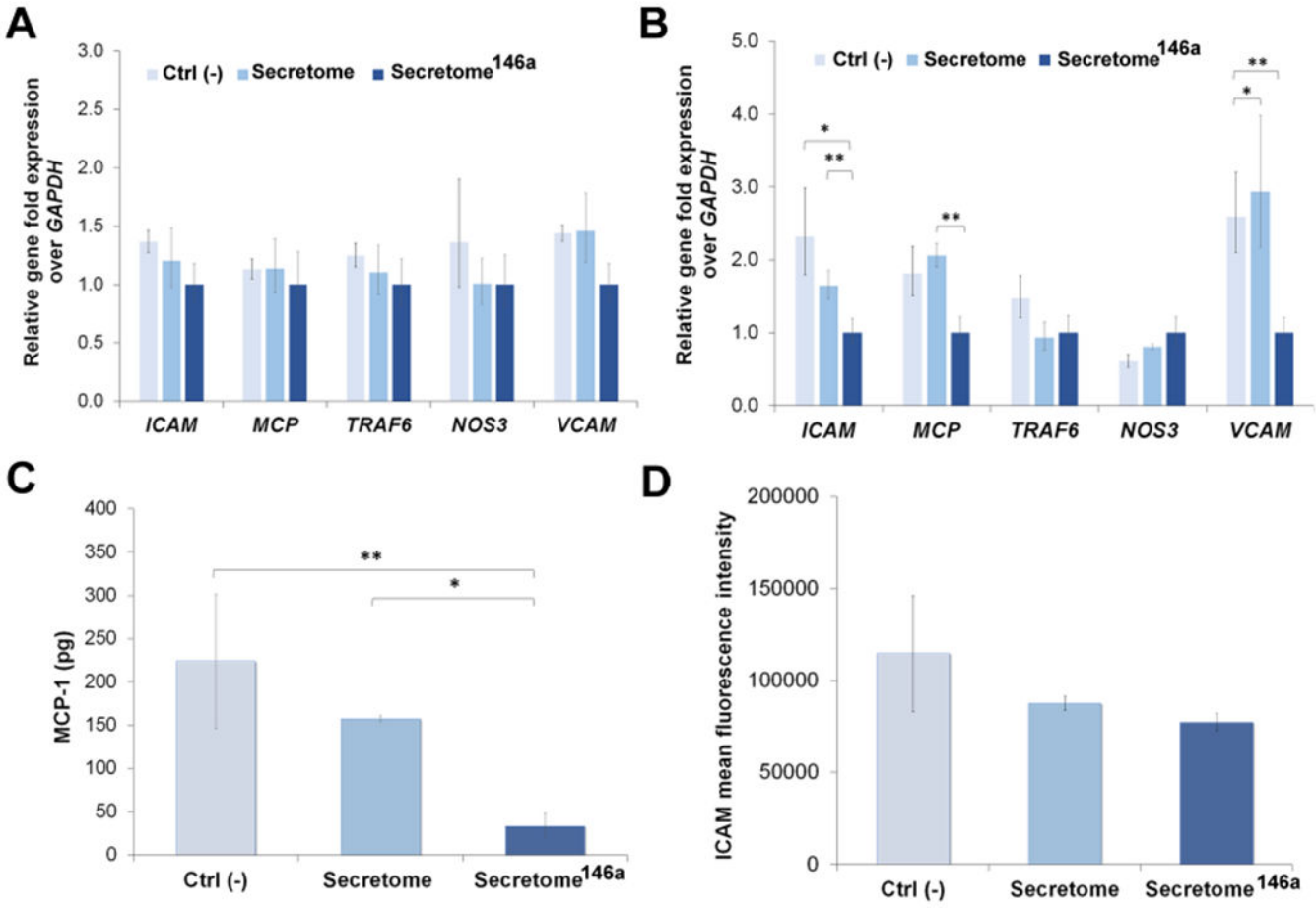

Figure 7.

Assessment of the anti-inflammatory response of the secretome^{146a}. (A, B) qPCR analysis of main genes involved in the inflammatory response of HUVECs upon exposure to IL-1β. Gene profiles of *ICAM*, *MCP-1*, *TRAF6*, *NOS3*, and *VCAM* were studied at 4 and 24 h. (C) Quantification of MCP-1 secreted by HUVECs after being exposed to IL-1β and subsequent treatment with the different types of the secretome. (D) FACs analysis reporting the mean fluorescent intensity of positive fluorescent stained HUVECs expressing the cellular molecular adhesion protein ICAM. Results are reported as mean ± deviation standard. *$p < 0.05$, **$p < 0.01$ ***$p < 0.001$.